



University of HUDDERSFIELD

University of Huddersfield Repository

Zhang, Xianlian, He, Xiaocong, Xing, Baoying, Zhao, Lun, Lu, Yi, Gu, Fengshou and Ball, Andrew

Influence of heat treatment on fatigue performances for self-piercing riveting similar and dissimilar titanium, aluminium and copper alloys

Original Citation

Zhang, Xianlian, He, Xiaocong, Xing, Baoying, Zhao, Lun, Lu, Yi, Gu, Fengshou and Ball, Andrew (2016) Influence of heat treatment on fatigue performances for self-piercing riveting similar and dissimilar titanium, aluminium and copper alloys. *Materials & Design*, 97. pp. 108-117. ISSN 0264-1275

This version is available at <http://eprints.hud.ac.uk/id/eprint/27387/>

The University Repository is a digital collection of the research output of the University, available on Open Access. Copyright and Moral Rights for the items on this site are retained by the individual author and/or other copyright owners. Users may access full items free of charge; copies of full text items generally can be reproduced, displayed or performed and given to third parties in any format or medium for personal research or study, educational or not-for-profit purposes without prior permission or charge, provided:

- The authors, title and full bibliographic details is credited in any copy;
- A hyperlink and/or URL is included for the original metadata page; and
- The content is not changed in any way.

For more information, including our policy and submission procedure, please contact the Repository Team at: E.mailbox@hud.ac.uk.

<http://eprints.hud.ac.uk/>

Influence of heat treatment on fatigue performances for self-piercing riveting similar and dissimilar titanium, aluminum and copper alloys

Xianlian Zhang¹⁾, Xiaocong He^{1),*}, Baoying Xing¹⁾, Lun Zhao¹⁾, Yi Lu¹⁾,
Fengshou Gu²⁾, Andrew Ball²⁾

1) Innovative Manufacturing Research Centre, Kunming University of Science and Technology,
Kunming, 650500, P. R. China

2) Centre for Efficiency and Performance Engineering, University of Huddersfield, Queensgate,
Huddersfield, HD1 3DH, UK.

Abstract: The fatigue performances of self-piercing riveting (SPR) joints connecting similar and dissimilar sheets of TA1 titanium alloy (TA1), Al5052 aluminium alloy (Al5052) and H62 copper alloy (H62) were studied in this paper. The specimens of similar TA1 sheets treated with stress relief annealing were prepared to investigate the influence of relief annealing on the mechanical properties of SPR joints. Fatigue tests were conducted to characterize the fatigue lives and failure modes of the joints. Scanning electron microscopy (SEM) was employed to determine the fatigue failure mechanisms of the joints. The results showed that stress relief annealing has an apparent impact on the fatigue performances but has little influence on the static strengths of the joints. For SPR joints in similar or dissimilar sheets, joints between similar TA1 sheets possess the best fatigue resistance, which are significantly higher than the joints in dissimilar sheets. And most of the joints failed in the rivet and the locked sheet through fatigue tests, except the joints between TA1 and Al5052, which failed only in the locked sheets.

Keywords: Self-piercing riveting, Sheet materials, Stress relief annealing, Fatigue performance, Fatigue failure mechanism

Corresponding author: Tel. : +86-871-65930928

E-mail address: x_he@kmust.edu.cn

1. Introduction

Due to increased environmental awareness and considerable pressure from energy shortages and environmental pollution, lightweight structures are regarded as an important means to enhance the competitiveness of products in industrial fields. Therefore, lightweight sheet materials are being increasingly used in aviation manufacturing, automobile manufacturing and other industries for energy conservation and the reduction of CO₂ emissions. However, most of these materials are difficult or impossible to join with resistance spot welding. Friction stir welding [1], laser welding [2], self-piercing riveting (SPR) [3], clinching [4] and adhesion [5] have been rapidly developed and widely applied in recent years as the main joining methods for these lightweight materials. One of these joining methods, SPR, is a cold-forming fastening process for point joining similar or dissimilar sheet materials with two or more layers. This method consumes a small amount of energy and results in high static and fatigue joint strengths. In addition, it does not require pre-drilled holes [6-8]. The SPR joint depends on a mechanical interlock. In the forming process, a semi-tubular rivet is pushed down by a punch into sheet materials fixed on a die. The die shape forces the rivet to flare inside the lower sheet to form a firm mechanical interlock [9]. As a result, the mechanical interlock is a key factor for joint strength. The quality of the joints is measured and assessed based on the rivet head height, the rivet spread and the remaining bottom thickness, which are normally used as quality criteria.

In the past few years, the mechanical properties of SPR joints and the SPR technique itself have been studied by many scholars. Xing et al. [10] investigated the mechanical behaviours of SPR joints with different distribution patterns, and found that the static strengths and fatigue lives of joints with multiple rivets were significantly better than those of joints with single rivets. The degree of improvement in strength for joints with the same number of rivets was different with different distribution patterns of the rivets. Kang et al. [11] aimed to evaluate the static and fatigue strengths of the joints using coach-peel, cross-tension and tensile-shear specimens with experimental tests and numerical analysis. Li et al. [12, 13] studied the influence of rivet centre to sheet edge distance on the quality, static behaviour and fatigue performance of double joints and concluded that edge distance was a dominant factor controlling lap-shear and coach-peel strength. Furthermore, edge distance had a large influence on lap-shear fatigue resistance but a less

significant influence on coach-peel fatigue resistance. The edge distance of 11.5 mm was the optimal distance to achieve higher joint strength and better fatigue performance. Su et al. [14] investigated the fracture and fatigue behaviours of self-piercing rivets and clinch joints in lap-shear specimens of 6111-T4 aluminium sheets based on experimental observations and examined the optical micrographs of both types of joints before and after failure under quasi-static and cyclic loading conditions.

Calabrese et al. [15, 16] recently conducted a long term salt spray corrosion test using steel/aluminium hybrid joints that were obtained via the SPR technique to evaluate mechanical degradation under these critical environmental conditions. The experimental results showed that the corrosion degradation phenomena significantly influenced both the performance and failure mechanisms of the joints. The joint configuration is a significant factor in the corrosion effect. Furthermore, they developed a theoretical model to forecast failure modes. Mori et al. [17] investigated the static and fatigue strengths of mechanically clinched, SPR and resistance spot welded joints in aluminium alloy sheets and compared the static and fatigue behaviours between the mechanical joining and metallurgical welding processes. The influence of resistance heating on dissimilar SPR joints with unequal thicknesses was studied systematically by Lou et al. [18]. They reported that SPR joints formed using rivet welding could obtain higher tensile-shear strengths than conventional SPR joints. He et al. [19] studied the mechanical properties of SPR joints between sheets of aluminium alloy and copper alloy and discovered that the joints in similar H62 copper alloy sheets exhibited the highest static strength and optimal fatigue performance, followed by joints between dissimilar sheets of Al5052 aluminium alloy and H62 copper alloy. Therefore, the SPR joint strength was obviously affected by the properties of the sheets. Di Franco et al. [20] researched the influence of the distance between rivets in SPR joints and showed that a joint separation of 60 mm between two rivets resulted in the best static behaviour in terms of tensile strength.

Mucha [21, 22] performed numerical modelling of solid self-piercing riveting (SSPR) and analysed the origin of the residue and its effect on rivet failure in the SSPR joints using the FEM method. It was concluded that moving the groove out of the rivet head base improved the groove filling with the lower sheet material, and the ridge width had no significant effect in terms of filling in more than one groove while joining DC01 material sheets. By increasing the SSPR rivet

forming force, the joint strength was increased. However, the pressing process with high forming force consumes a lot of energy and produces significant residual stress in the rivet. Haque et al. [23] developed a simple geometrical method to calculate rivet flaring without having to cross-section a joint. It is a nondestructive testing method for determining rivet flaring based on the characteristic force-displacement curve and could be a very useful tool in joint product development and process optimisation. Using experimental and numerical methods, Hoang et al. [24] studied the structural behaviour of the T-components made by joining two aluminium extrusions using aluminium self-piercing rivets. They found that the maximum force level of the components with aluminium rivets was approximately 5-8% lower than that of the components with steel rivets and that the ductility of the T-components based on aluminium rivets was approximately 50% less than that based on steel rivets. The purpose of Grujicic's research [25] was to develop a three-step computational procedure to establish dependence of the mechanical properties of the SPRs on the SPR process parameters. The procedure involved finite-element modelling and simulations of the SPR process and virtual testing of the resulting SPR joints under different types of loading.

However, no investigation of the fatigue properties of SPR joints in titanium alloys has been published until now. Titanium alloys have been widely used in the aerospace, maritime, nuclear power, petrochemical, and construction industries owing to their excellent comprehensive performance, including good deformability, low density, high specific strength, excellent corrosion resistance and high temperature strength retention [26-28]. SPR joints between titanium alloy sheets and other lightweight alloys have also been extensively used in industrial fields. In the previous paper by He et al. [29], the static strength of SPR joints in similar and dissimilar TA1 titanium alloy (TA1) sheets was studied. This work was conducted to study the effects of heat treatment on fatigue performances of SPR joints in TA1, aluminium alloy (Al5052) and copper alloy (H62). Fatigue load-fatigue life curves were obtained via tension-tension fatigue tests to characterise the fatigue properties of different types of joints. Moreover, the typical fracture interfaces were analysed by scanning electron microscopy (SEM). The conclusions could provide a reference for further research on SPR joints in titanium alloys.

2 Experimental procedure

2.1 Materials

The materials used in this study were TA1 titanium alloy sheets, Al5052 aluminium alloy sheets and H62 copper alloy sheets with dimensions of 110 mm × 20 mm × 1.5 mm. All sheets were cut along the rolling direction. The chemical compositions of the sheet materials are listed in Table 1. For better analysis about the SPR joints with stress relief annealing, TA1 sheets annealed at 540 °C (TA1A) were made. To obtain the sheet mechanical properties, material tests were conducted using an MTS 634.31F-24 extensometer with a 20 mm gauge length on an MTS servo hydraulic test machine. The mechanical properties of the TA1, Al5052, H62 and TA1A sheets are shown in Table 2. The stress-strain curves at a constant crosshead speed of 5 mm/min are shown in Fig. 1.

Table 1. Chemical compositions of the sheet materials (%)

Material	Fe	C	N	H	O	Ti
TA1	0.02	0.01	0.01	0.001	0.08	Rest
Material	Si	Cu	Mg	Zn	Mn	Al
Al5052	0.25	0.1	2.2	0.1	0.1	Rest
Material	Zn	Fe	Pb	P	Cu	
H62	36.8	0.15	0.08	0.01	Rest	

Table 2. Mechanical properties of the sheet materials

Material	Young's modulus (GPa)	Tensile strength (MPa)	Yield strength (MPa)	Elongation (%)
TA1	81.8	406.7	371.8	43
Al5052	69.5	229.9	211.5	14
H62	110.0	424.5	340.3	37
TA1A	111.2	494.8	426.0	33

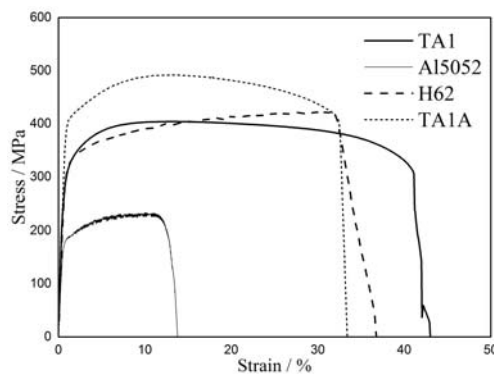


Fig. 1. Stress-strain curves for sheet materials

2.2 Specimens preparation

The specimen geometry is presented in Fig. 2. All specimens were produced with a rivet and a flat bottom die on a RIVSET VARIO-FC servo-driven riveting machine by Böllhoff (Germany). Both the rivet and the die were fabricated from high-strength steel and were supplied by Böllhoff GmbH & Co. The dimensions of the rivet and the die are shown in Fig. 3. Considering the conclusions of He et al. [29], the SPR joints of dissimilar sheets with TA1 as upper sheets, which had a better load-bearing capacity than SPR joints with TA1 as lower sheets, were selected for the study. To make it easy to describe different SPR joints, the following nomenclature is used:

- STT joint: SPR joint in similar TA1 sheets;
- TTA joint: SPR joint in similar TA1 sheets with stress relief annealing;
- STA joint: SPR joint between sheets of TA1 (upper sheet) and Al5052 (lower sheet);
- STH joint: SPR joint between sheets of TA1 (upper sheet) and H62 (lower sheet).

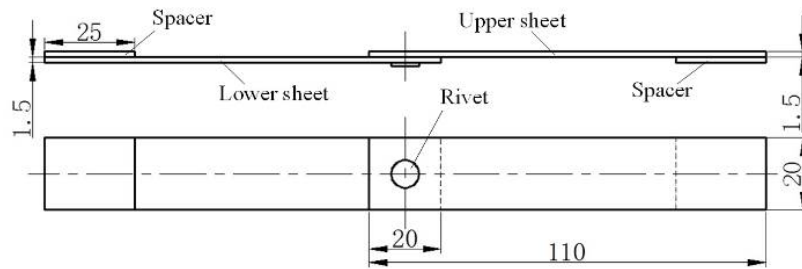


Fig. 2. Specimen geometry

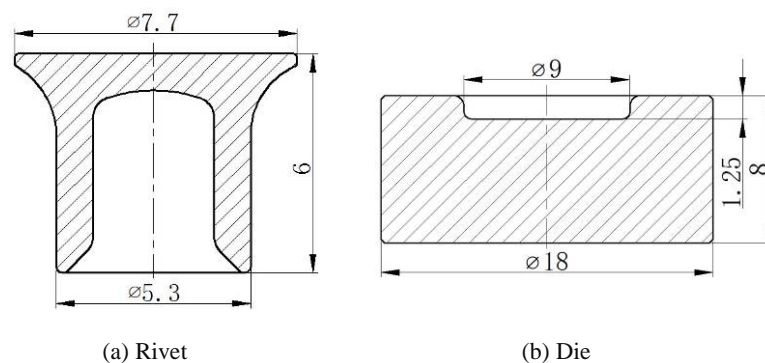


Fig. 3. Dimensions of the rivet and the die

To increase the material formability, TA1 sheets with STT, TTA and STH joints were heated to the maximum heating temperature 700 °C by an oxyacetylene flame gun on a heating platform as shown in Fig. 4. The heating temperature can be controlled by an infrared

thermometer. The SPR processes were produced immediately after heat treatment. To obtain satisfied SPR joints, different types of SPR joints were made under different riveting pressures which come from preliminary SPR tests for different materials combinations. The quality of the specimens was monitored by an online window monitoring system in the riveting equipment during the SPR processes. The monitoring was carried out by measuring the actual SPR setting force through a force sensor and the punch travel through a position sensor and generating a force-travel curve for one SPR joint [9]. The force-travel curves should be almost identical under the same working conditions for different types of joints. This indicates that the quality of corresponding joints is good. Based on the online window monitoring system, all specimens were judged as qualified. The satisfied joining parameters for different types of SPR joints were shown in Table 3.

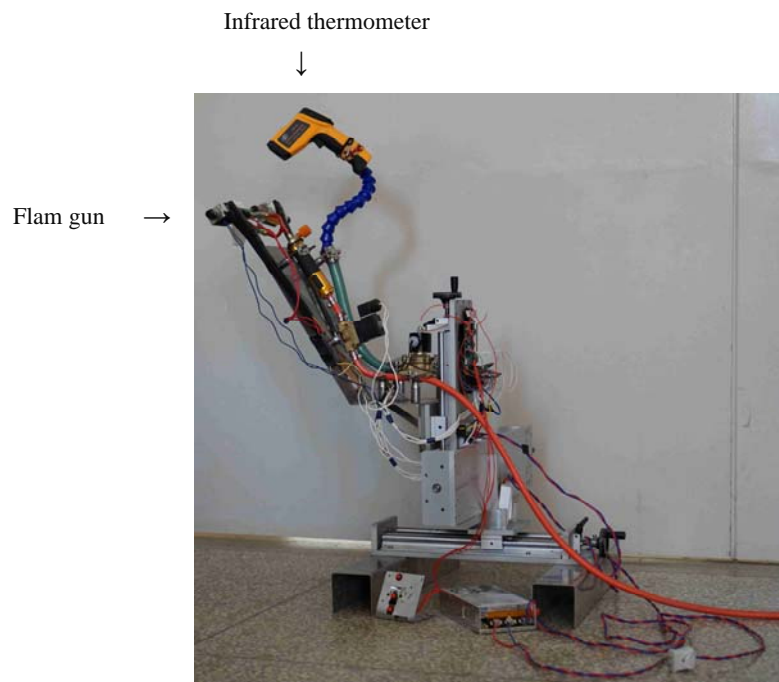


Fig. 4. Heating platform

Table 3. Joining parameters for different SPR joints

Joint	Punch travel (mm)	Material check pressure (bar)	Riveting pressure (bar)	Compressing pressure (bar)
STT	131.40	50	220	110
TTA	131.40	50	220	110
STA	131.20	50	220	110
STH	131.20	50	195	110

SPR is a cold-forming process, and the fatigue performance of the joints is significantly influenced by the stress concentration and residual stress in the process of plastic deformation during the joining process. One of the purposes of annealing is to reduce or eliminate the internal stress in the cold-forming process [30]. To investigate the influence of annealing on the fatigue performance of SPR joints, fifty STT joints were made. Twenty-five of these joints, called TTA joints, were chosen randomly and annealed at 540 °C for 1 h in a quartz annealing furnace system. There were twenty-five of each type of joint, ten of which were selected randomly for the static tests, and the remainder were prepared for the fatigue tests. The STT, TTA, STA and STH joints are shown in Fig. 5.

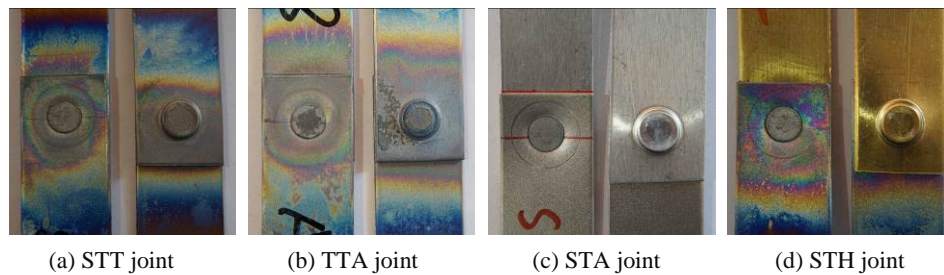


Fig. 5. Different types of SPR joints

2.3 Static tests

The static tests were conducted on an MTS servo hydraulic testing machine using the tensile-shear mode. Spacers with dimensions of 30 mm × 20 mm × 1.5 mm were glued on both ends of the specimens to reduce the influence of additional bending and to centralize the load. The tests were performed with a constant displacement rate of 5 mm/min. Ten tests were conducted for each type of joint. The different failed specimens and close-up images for the static tests are shown in Fig. 6.

2.4 Fatigue tests

According to the static test results, the average peak loads of the STT joints, TTA joints, STA joints and STH joints were 6.807 kN, 6.853 kN, 5.477 kN and 6.076 kN, respectively. The parameters of the fatigue tests were determined based on the average peak loads. For better fatigue performances, different type of SPR joints has different load levels in fatigue tests. In present study, different load levels for different type of SPR joints were determined by preliminary fatigue tests.

The load-controlled cyclic fatigue tests were carried out on the MTS servo hydraulic testing machine using a sine waveform in the tension-tension mode. A load ratio $R = 0.1$ and a frequency $f = 10$ Hz were employed for all specimens. Each test was run until 2 million cycles were attained or visible failure occurred. Three load levels of 50%, 30% and 25% were tested for the STT joints and TTA joints, three load levels of 70%, 35% and 20% were tested for the STA joints, and three load levels of 35%, 30% and 25% were tested for the STH joints. For all types of joints, the three specimens tested at each load level were randomly selected from the fifteen prepared joints. To reduce the bending of the sheets and ensure straight-line load paths, spacers with dimensions of 30 mm \times 20 mm \times 1.5 mm were glued to both ends of all specimens in the clamping area. Fig. 7 shows the different failed specimens for the fatigue tests.

3 Results and analysis

3.1 Static test results

One force-displacement curve for each type of joint (the one that was closest to the average peak load) was chosen, and these curves are shown in Fig. 8 to facilitate comparison.

To examine the rationality of the test data, the normal hypothesis tests were performed using MATLAB 2014b. The results show that all peak loads of different SPR joints follow normal distributions. Thus, the Grubbs criterion was used to eliminate outliers, and it was found that there were no outliers in the data on the four types of joints. Fig. 9 shows the average peak loads of the different joints.

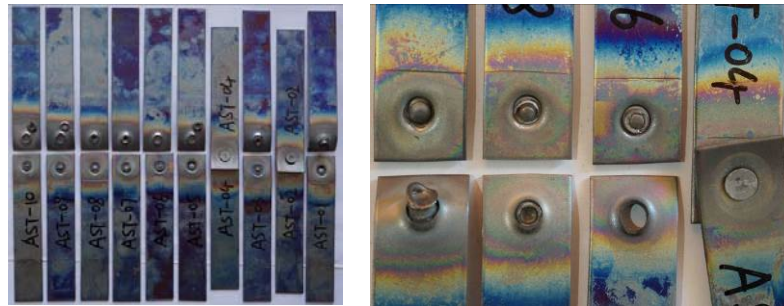
Fig. 9 shows that the average peak load of the STT joints (6.807 kN) is very similar to that of the TTA joints (6.853 kN). Therefore, stress relief annealing has little influence on the static strength of SPR joints. Among the joints without stress relief annealing, the STT joints possessed the highest average peak load; the STH joints at 6.076 kN were slightly higher than the STA joints at 5.477 kN. For the SPR joints in the same upper sheet, the yield strength of the lower sheet is a key factor in the static strength of the joints.

From Fig. 6, it is obvious that different types of SPR joints have different failure modes. For STT joints, nine specimens failed because the rivet fractured, and one specimen was not completely separated. For the TTA joints, seven specimens failed because the rivet fractured, two specimens were not completely separated, and only one failed because the rivet was pulled from

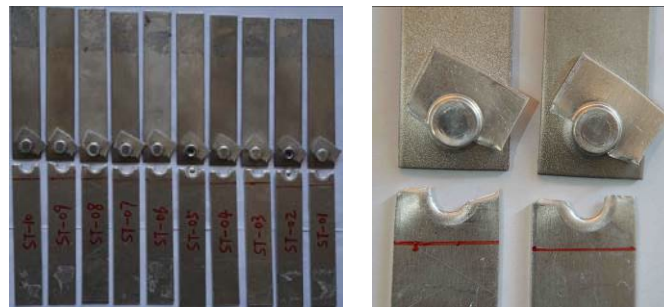
the lower sheet. However, all failures of the STA joints were caused by a fracture of the locked sheet. For the STH joints, rivets were broken for seven specimens, and three specimens were not completely separated. Consequently, it is easy to discover that the strength gap between the upper and lower sheets has a significant influence on the SPR joint failure mode.



(a) Failed STT joint



(b) Failed TTA joint



(c) Failed STA joint



(d) Failed STH joint

Fig. 6. Different failed SPR joints for the static tests

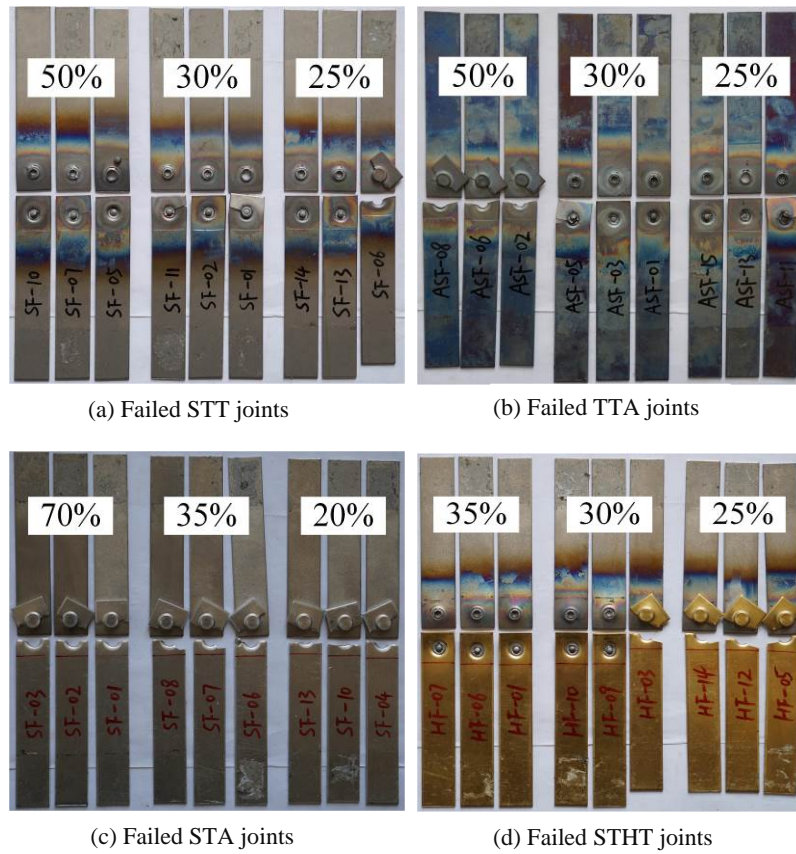


Fig. 7. Different failed SPR joints for the fatigue tests

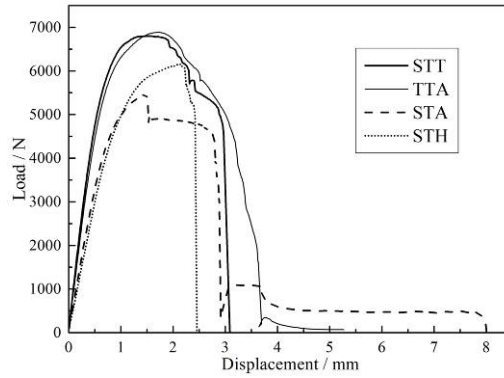


Fig. 8. Force-displacement curves of different SPR joints

3.2 Fatigue life

The fatigue data and the fatigue load-fatigue life ($F-N$) curves fitted by the least square method are presented in Fig. 10. For SPR joints in similar TA1 sheets, the fatigue strength is shown in Fig. 10(a), and the calculated linear equations for the STT and TTA joints are $F = 8.244 - 1.085 \log(N)$ and $F = 9.822 - 1.374 \log(N)$, respectively. Fig. 10(a) shows that the crossover

point of these two $F-N$ curves is (5.479, 2.297). When the maximum fatigue load was higher than approximately 2.3 kN, the TTA joints exhibited a longer fatigue life than the STT joints. As the maximum fatigue load dropped below 2.3 kN, the fatigue life of the STT joints began to exceed that of the TTA joints, and the gap between the two curves grew rapidly. However, for the specimens tested at load levels of 50% (3.4 kN) and 30% (2.0kN), the STT joint fatigue lives of 34,289 ($\log(N)=4.5$) and 312,478 ($\log(N)=5.5$) cycles were significantly lower than the TTA joint fatigue lives of 45,697 ($\log(N)=4.7$) and 487,898 ($\log(N)=5.7$) cycles. As the load level decreased to 25% (1.7 kN), a huge gap between the STT joints and TTA joints occurred, resulting in average fatigue lives of 1,327,932 ($\log(N)=6.1$) and 679,858 ($\log(N)=5.8$) cycles, respectively. It can be concluded that the fatigue strength of the SPR joints in similar TA1 sheets could not be improved by relief annealing but could be greatly decreased in the low load and long life range, whereas it could be enhanced obviously in the short life zone. In the middle life range, no clear difference emerged.

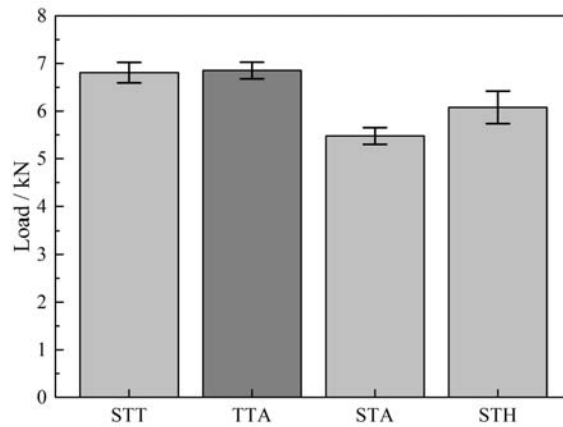


Fig. 9. Average peak loads of different SPR joints

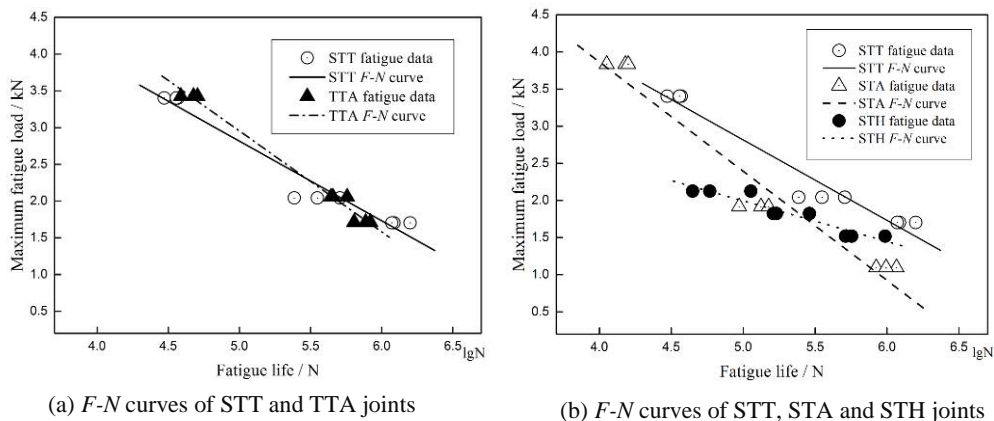


Fig. 10. $F-N$ curves of different SPR joints

The fatigue resistances of SPR joints between dissimilar sheets are shown in Fig. 10(b). The calculated linear equations of the STA and STH joints are $F = 9.750 - 1.471 \log(N)$ and $F = 4.739 - 0.549 \log(N)$, respectively. In the short life range, the STA joints exhibited a higher fatigue strength than the STH joints with 14,089 ($\log(N)=4.1$) cycles, which was very close to the number of cycles run for the STT joints at the same fatigue load of approximately 3.8 kN. Moreover, the STH joints had an average cycle number of 72,102 ($\log(N)= 4.9$) at a fatigue load of approximately 2.1 kN. In the middle life zone, 125,534 ($\log(N)= 5.1$) cycles and 206,935 ($\log(N)= 5.3$) cycles were run for the STA joints at approximately 1.9 kN and the STH joints at approximately 1.8 kN; these cycle performances were significantly lower than those for the STT joints. As the fatigue load decreased, the gap between the fatigue resistances of the STH and STT joints gradually decreased. The STH joints, which had lifetimes of 684,255 ($\log(N)= 5.8$) cycles at approximately 1.5 kN, were obviously superior to the STA joints, and an average of 996,440 ($\log(N)= 6.0$) cycles were run for the STA joints at nearly 1.1 kN. As shown in Fig. 10(b), the crossover point of the STA and STH $F-N$ curves is (5.435, 1.755). Consequently, it could be concluded that when the lower sheet was changed from H62 to A15052, the fatigue resistance improved when the fatigue load was greater than 1.8 kN and decreased when the fatigue load was below 1.8 kN. In the short life range, the fatigue resistances of the STA and STT joints were almost identical and distinctly superior to that of the STH joints. However, in the long life range, there was little difference in the fatigue strengths of the STH and STT joints, which were significantly higher than those of the STA joints. Moreover, in the middle life range, the STT joints were better than the STA and STH joints in terms of fatigue resistance.

3.3 Fatigue failure mode

During the tensile-shear tests, the STT and TTA joints failed with the rivet being broken or pulled out from the locked sheet, the STA joints failed in the locked sheet, and nearly all STH joints failed with the rivet being pulled out from the pierced sheet or the locked sheet [18]. However, as presented in Fig. 7, the failures during the fatigue tests were quite different. For the STT and TTA joints, almost all specimens failed by rivet fracture. For the STA joints, all specimens failed in the locked sheet. For the STH joints, five failed by rivet fracture, and the other failed in the locked sheet.

The failure modes of the different SPR joints are listed in Table 4. It can be observed from Fig. 7(a) that the rivet could be regarded as a vulnerable point in STT joints which were not subject to relief annealing. At the load level of 50%, the failure regions of the joints with similar TA1 sheets were transferred from the rivet to the locked sheet through relief annealing (see Fig. 7(b)). Because the interlock is affected by the rivet, it can be concluded that the fatigue strength of the TTA joints is improved by relief annealing in the high load and short life range. For the load level of 30%, all specimens failed in the rivets for both STT and TTA joints. The failure mode of the locked sheet fracture occurred again in the STT joints at the load level of 25% (see Fig. 7(a)). As a result, the fatigue strength was reduced through relief annealing in the low-load and long-life range. According to the above discussions, the relationships between failure modes are absolutely consistent with the previously discussed conclusions regarding the fatigue lives.

For SPR joints in dissimilar sheets, all STA joints failed in the locked sheets, which were broken during the fatigue tests at load levels of 70%, 35% and 20%. For the STH joints, at load levels of 35% and 30%, five specimens fractured in the rivet, and only one specimen failed in the locked sheet. As the load level dropped to 25%, the locked sheets were broken for all specimens. Overall, considering the data in Table 4 and Fig. 10, it can be inferred that for the specimens in similar or dissimilar sheets at the same fatigue load, the fatigue resistances of the joints that failed in the locked sheet were indeed superior to those of the joints that failed because of rivet fracture. When different types of joints failed in the same mode, the fatigue resistance was directly determined by the properties of the upper or lower sheets.

Table 4. Failure modes of different SPR joints.

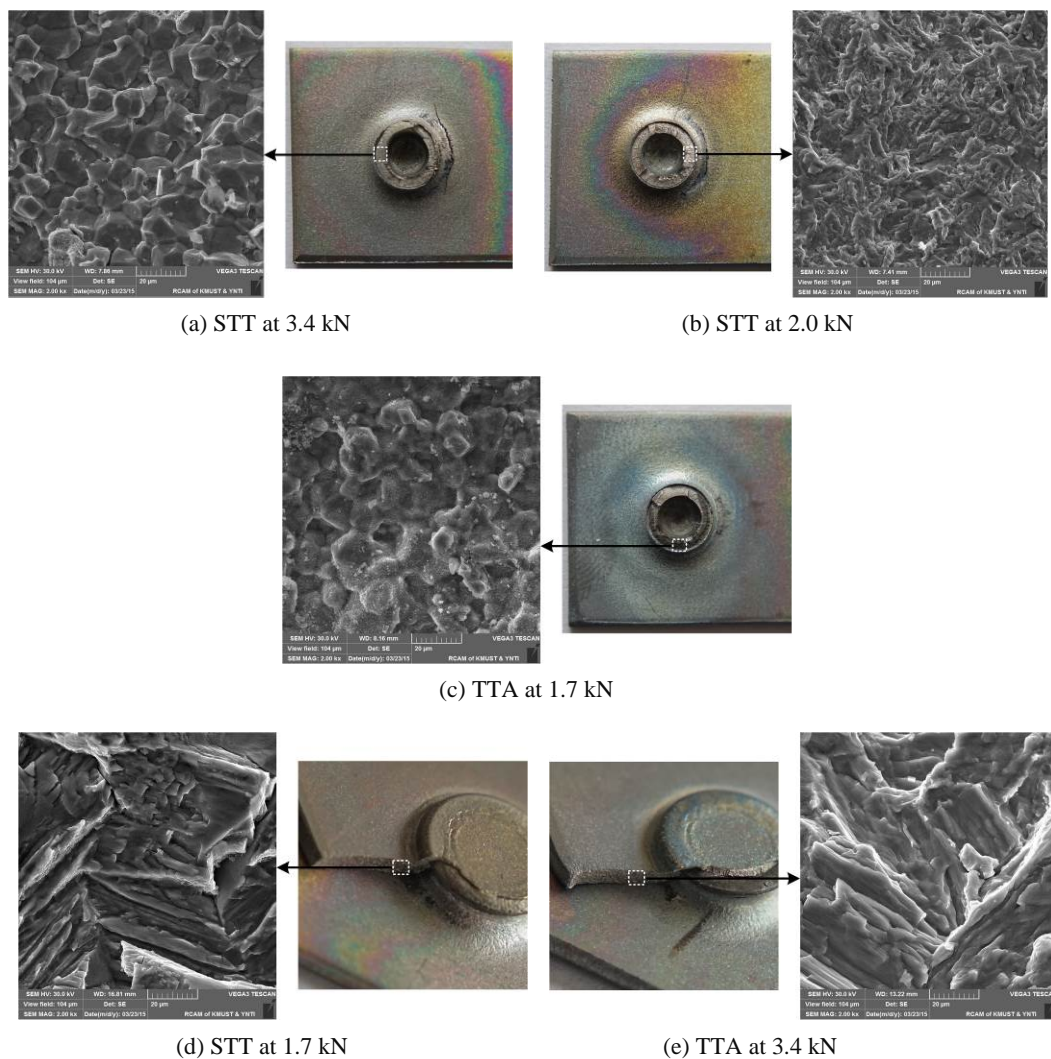
Load level / Maximum load (kN)	STT joints	Load level / Maximum load (kN)	TTA joints
50% / 3.4	Rivet fracture	50% / 3.4	Locked sheet fracture
30% / 2.0	Rivet fracture	30% / 2.0	Rivet fracture
25% / 1.7	2/3 rivet fracture & 1/3 locked sheet fracture	25% / 1.7	Rivet fracture
Load level / Maximum load (kN)	STA joints	Load level / Maximum load (kN)	STH joints
70% / 3.8	Locked sheet fracture	35% / 2.1	Rivet fracture
35% / 1.9	Locked sheet fracture	30% / 1.8	2/3 rivet fracture & 1/3 locked sheet fracture
20% / 1.1	Locked sheet fracture	25% / 1.5	Locked sheet fracture

3.4 Fatigue failure mechanism

Based on the above discussions, there were two failure modes for each type of SPR joints, except for STA joints. Thus, after the fatigue tests, two typical fracture surfaces for the two failure modes of STT, TTA and STH joints and one typical fracture surface for STA joints were randomly selected for examination using a scanning electron microscope (SEM, TESCAN: VEGA3 SCAN) to study the fatigue failure mechanisms of the joints.

3.4.1 For STT and TTA joints

The different macroscopic fracture surfaces and SEM images of the STT and TTA joints are shown in Fig. 11. Through SEM examination, it was found that the SEM images of the rivet fracture surfaces at the fatigue loads of 2.0 kN and 1.7 kN for the STT and TTA joints were highly similar. Accordingly, the fracture surface of STT joints at 2.0 kN and the fracture surface of the TTA joints at 1.7 kN are selected, and their SEM images are shown.



As shown in Fig. 11(a), it can be observed from the macroscopic fracture surface that the STT specimens at 3.4 kN generally failed in the rivet, and fatigue cracks occurred near the pierced hole in the upper sheet. The microscopic fatigue fracture surface of the STT specimen at 3.4 kN was magnified 2000 times. Crystal surfaces that look like sugar crystals can be observed clearly; this fracture mode is brittle intergranular fracture. However, the TTA joints failed due to locked sheet fracture at 3.4 kN. As shown in Fig. 11(e), the fatigue cracks were generally initiated near the rivet shank in the lower sheet and then propagated in the transverse direction until the lower sheet broke because of interlock damage. In the SEM image, the fracture surface can be observed with brittle fatigue striations that possess the predominant feature of the cleavage river pattern. Compared with the microscopic fracture surface of the locked sheet for the STT specimens treated without relief annealing, as shown in Fig. 11(d), the microscopic fracture surfaces of the STT specimens are not as smooth as those of the TTA specimens. Moreover, STT shows a typical feather pattern in the fatigue source region. As a result, it can be inferred that, in the failure process of the STT specimens, the fatigue cracks initiated at locations near the rivet shank in the locked sheet and propagated in the vertical and transverse directions to the nearest edge and then along the circular bulge to the other edge of the locked sheet, resulting in interlock damage. Fig. 11(b) and Fig. 11(c) show the fracture interfaces of the STT specimens at 2.0 kN and the TTA specimens at 1.7 kN, respectively. Small fatigue stripes can be observed in the SEM image shown in Fig. 11(b), which are the typical characteristics of the fatigue source region and the ductile fatigue fracture. The feature that can be observed in Fig. 11(c) is similar to that of Fig. 11(a). Nevertheless, the grain boundaries became extremely weak due to the influence of relief annealing, and the initiation and propagation of the cracks were carried out in a low-energy configuration. These characteristics also indicate brittle intergranular fracture.

3.4.2 For STA and STH joints

According to the results of the SEM analysis, the fatigue failures caused by the locked sheet fracture and the failure mechanisms of the STA and STH joints were almost the same. The macroscopic fatigue fracture surfaces of the STA specimens that failed in the locked sheet at 1.9 kN and the STH specimens that failed in the rivet at 2.1 kN are discussed in detail and shown in Fig. 12.

Fig. 13(a), (b), (c) and (d) are enlarged images of the locations marked A, B, C and D in Fig. 12(a), respectively. It can be observed from Fig. 12(a) that the specimens failed because the locked sheet fractured without the interlock being damaged. Fig. 13(a) shows the microscopic structure of the crack initiation locations. The like-cleavage tongue patterns, which are typical characteristics of fatigue fracture source regions, revealed that cracks initiated near the rivet shank in the locked sheet and propagated in the sheet thickness and transverse direction indicated by an arrow. As shown in Fig. 13(b), fatigue stripes can be clearly observed, which is representative of the second stage of fatigue crack diffusion. The black debris caused by fretting wear on the interface between the rivet and the locked sheet can be found easily, as marked by a circle in Fig. 13(c). Fig. 13(d) shows a microscopic image of the other side of the fracture surface of the locked sheet, on which many dimples can be clearly observed. These dimples are typical features of ductile fracture. Consequently, it is believed that the fatigue cracks initiated adjacent to the rivet shank in the locked sheet because of the fretting wear and propagated initially along the sheet thickness direction and subsequently perpendicular to the loading direction to the nearest sheet edge and then along the circular bulge of the lower sheet to the other side of the sheet. Finally, when the residual structure could not bear the fatigue load applied, sudden fracture occurred. As observed in Fig. 12(b), the STH specimens failed only by rivet fracture without any damage in the lower sheet. The SEM image of the rivet fracture surface is shown in Fig. 13(e), from which the fatigue striations can be obviously observed. This characteristic belongs to the ductile fatigue fracture. It can be observed from the direction marked by an arrow in Fig. 13(e) that fatigue cracks propagated from the outside of the rivet to the inside.

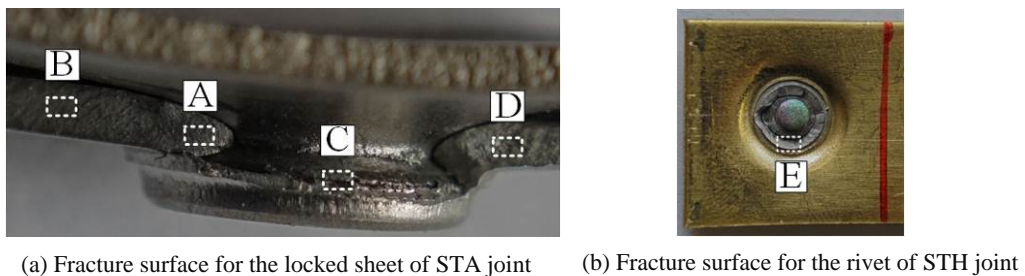
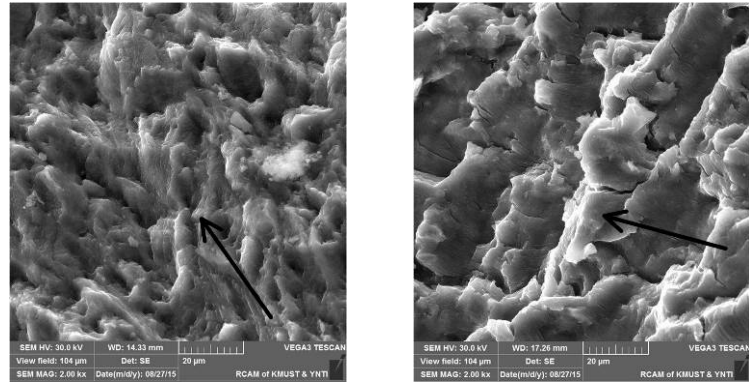
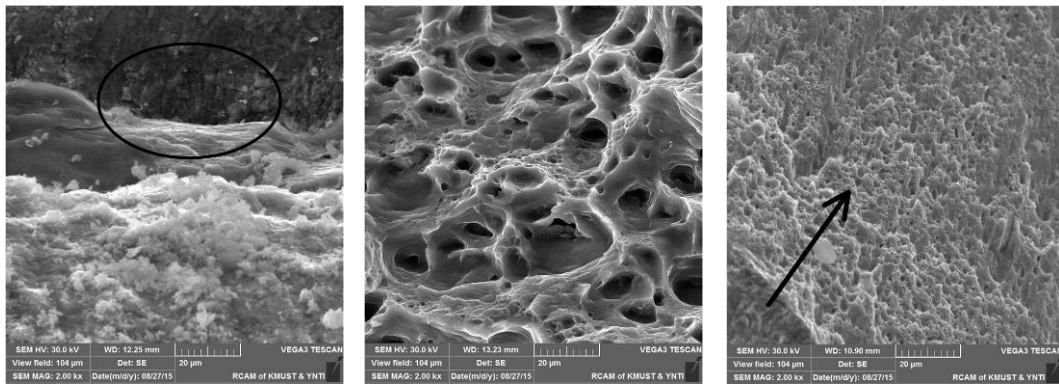


Fig. 12. Macroscopic fracture surfaces of STA and STH specimens



(a) Enlarged area: A

(b) Enlarged area: B



(c) Enlarged area: C

(d) Enlarged area: D

(e) Enlarged area: E

Fig. 13. SEM images of fracture surface for STA and STH specimens

4 Conclusion

In this paper, the fatigue performances of SPR joints between similar and dissimilar sheets of TA1, Al5052 and H62 were studied. To investigate the influence of relief annealing on the mechanical properties of SPR joints, similar sheets were fabricated with and without relief annealing. The fatigue lives, failure modes and fatigue failure mechanisms of the tested specimens were discussed to characterise the fatigue performances of the SPR joints. The major conclusions of this research can be listed as follows:

1. Relief annealing had an apparent impact on the fatigue performances of the SPR joints but little influence on the static strengths of the STT and TTA joints with peak loads of 6.807 kN and 6.853 kN, respectively. The fatigue strength of the TTA joints treated with relief annealing was greatly reduced in the long life range but enhanced obviously in the short life range. Owing to the influence of relief annealing, the failure modes of the joints treated with relief annealing transferred from a rivet fracture to a locked sheet fracture at the maximum fatigue load of 3.4 kN,

and all TTA joints failed due to rivet failure at loads of 2.0 kN and 1.7 kN.

2. In terms of fatigue life, the STA joints were almost equivalent to the STT joints, and they were distinctly superior to the STH joints in the short life range. In the long life range, there was little difference between the STH joints and the STT joints, which were significantly higher than the STA joints. In the middle life range, the STT joints were obviously better than the STA and STH joints.

3. The fatigue failure modes of the joints were quite different. Most STT joints failed by rivet fracture; only one sample at the fatigue load of 1.7 kN failed by locked sheet fracture. All STA joints failed by locked sheet fracture. The STH joints mainly failed in the rivet at fatigue loads of 2.1 kN and 1.8 kN, and all failed in the locked sheet at 1.5 kN.

4. The fatigue failure mechanisms of the same failure modes possessed some similarities. Almost all rivet fracture surfaces of the STT specimens at 2.0 kN and 1.7 kN and of the STH specimens were ductile fatigue fractures. The other rivet fracture surfaces of the specimens were brittle fatigue fractures. In addition, for all microscopic fracture surfaces of the locked sheets for different SPR joints, it is believed that the fatigue cracks initiated adjacent to the rivet shank in the locked sheets due to fretting wear and propagated initially in the vertical direction, and then perpendicular to the loading direction to the nearest sheet edge and finally along the circular bulge of the lower sheet to the other side of the sheet. The lower sheets were completely broken when the residual structure could not sustain the applied fatigue loads.

Acknowledgments

This research is supported by National Natural Science Foundation of China (Grant No. 51565023, 51565022).

References

- [1] He X, Gu F, Ball A. A review of numerical analysis of friction stir welding. *Prog Mater Sci* 2014;65:1-66.
- [2] Cao X, Jahazi M. Effect of welding speed on butt joint quality of Ti-6Al-4V alloy welded using a high-power Nd:YAG laser. *Optic Laser Eng* 2009; 47(11): 1231-41.
- [3] Mucha J. The analysis of lock forming mechanism in the clinching joint. *Mater Des* 2011;

32(10):4943-54.

- [4] Lambiase F. Influence of process parameters in mechanical clinching with extensible dies. *Int J Adv Manuf Technol* 2012;66:2123-31.
- [5] He X. Influence of boundary conditions on stress distributions in a single-lap adhesively bonded joint. *Int J Adhes Adhes* 2014;53:34-43.
- [6] Wood PKC, Schley CA, Williams MA, Rusinek A. A model to describe the high rate performance of self-piercing riveted joints in sheet aluminum. *Mater Des* 2011; 32: 2246–59.
- [7] Huang L, Bonnen J, Lasecki J, Guo H, Su X. Fatigue and fretting of mixed metal self-piercing riveted joint. *Int J Fatigue* 2016; 83: 230-9.
- [8] Mori K, Abe Y, Kato T. Self-pierce riveting of multiple steel and aluminum alloy sheets. *J Mater Process Technol* 2014;214(10):2002-8.
- [9] He X, Xing B, Zeng K, Gu F, Ball A. Numerical and experimental investigations of self-piercing riveting. *Int J Adv Manuf Technol* 2013;69:715-721.
- [10] Xing B, He X, Zeng K, Wang Y. Mechanical properties of self-piercing riveted joints in aluminum alloy 5052. *Int J Adv Manuf Technol* 2014;75:351-361.
- [11] Kang S, Kim H. Fatigue strength evaluation of self-piercing riveted Al-5052 joints under different specimen configurations. *Int J Fatigue* 2015;80:58-68.
- [12] Li D, Han L, Thornton M, Shergold M. Influence of edge distance on quality and static behaviour of self-piercing riveted aluminium joints. *Mater Des* 2012;34:22-31.
- [13] Li D, Han L, Thornton M, Shergold M. Influence of rivet to sheet edge distance on fatigue strength of self-piercing riveted aluminium joints. *Mater Sci Eng A* 2012;558:242-252.
- [14] Su Z, Lin P, Lai W, Pan J. Fatigue analyses of self-piercing rivets and clinch joints in lap-shear specimens of aluminum sheets. *Int J Fatigue* 2015;72:53-65.
- [15] Calabrese L, Proverbio E, Pollicino E, Galtieri G, Borsellino C. Effect of galvanic corrosion on durability of aluminium/steel self-piercing rivet joints. *Corros Eng Sci Technol* 2015;50(1):10-17.
- [16] Calabrese L, Proverbio E, Pollicino E, Galtieri G, Borsellino C. Failure behaviour of SPR joints after salt spray test. *Eng Struct* 2015;82:33-43.
- [17] Mori K, Abe Y, Kato T. Mechanical of superiority of fatigue strength for aluminium alloy sheets joined by mechanical clinching and self-pierce riveting. *J Mater Process Technol*

2012;212:1900-1905.

- [18] Lou M, Li Y, Wang Y, Wang B, Lai X. Influence of resistance heating on self-piercing riveted dissimilar joints of AA6061-T6 and galvanized DP590. *J Mater Process Technol* 2014;214:2119-2126.
- [19] He X, Zhao L, Deng C, Xing B, Gu F, Ball A. Self-piercing riveting of similar and dissimilar metal sheets of aluminum alloy and copper alloy. *Mater Des* 2015;65:923-933.
- [20] Di Franco G, Fratini L, Pasta A. Influence of the distance between rivets in self-piercing riveting bonded joints made of carbon fiber panels and AA2024 blanks. *Mater Des* 2012;35:342-349.
- [21] Mucha J. The numerical analysis of the effect of the joining process parameters on self-piercing riveting using the solid rivet. *Arch Civ Mech Eng* 2014;14(3):444-454.
- [22] Mucha J. The failure mechanics analysis of the solid self-piercing riveting joints. *Eng Fail Anal* 2015; 47(PA):77-88.
- [23] Haque R, Williams N, Blacket S, Durandet Y. A simple but effective model for characterizing SPR joints in steel sheet. *J Mater Process Technol* 2015; 223:225-231.
- [24] Hoang NH, Hanssen AG, Langseth M, Porcaro R. Structural behaviour of aluminium self-piercing riveted joints: An experimental and numerical investigation. *Int J Solids Struct* 2012; 49(23-24):3211-3223.
- [25] Grujicic M, Snipes J, Ramaswami S, Abu-Farha F. Process modeling, joint-property characterization and construction of joint connectors for mechanical fastening by self-piercing riveting. *Multidiscip Model Mater Struct* 2014; 10(4):631-658.
- [26] Banerjee D, Williams J. Perspectives on titanium science and technology. *Acta Mater* 2013; 61:844-879.
- [27] Li G, Li Y, Wang F, Wang H. Microstructure and performance of solid TC4 titanium alloy subjected to the high pulsed magnetic field treatment. *J Alloys Compd* 2015; 644:750-756.
- [28] Lee W, Lin C. Plastic deformation and fracture behaviour of Ti-6Al-4V alloy loaded with high strain rate under various temperatures. *Mater Sci Eng A* 1998; 241:48-59.
- [29] He X, Wang Y, Lu Y, Zeng K, Gu F, Ball A. Self-piercing riveting of similar and dissimilar titanium sheet materials. *Int J Adv Manuf Technol* 2015; 80:2105–2115.
- [30] Zhang N, Wang W, Cao X, Wu J. The effect of annealing on the interface microstructure and

mechanical characteristics of AZ31B/AA6061 composite plates fabricated by explosive welding. Mater Des 2015; 65:1100-1109.